The FEBS Journal
FEBS PRESS science publishing by scientists

A stereospecific carboxyl esterase from *Bacillus coagulans* hosting non-lipase activities within a lipase-like fold

Journal:	*The FEBS Journal*
Manuscript ID	Draft
Manuscript Type:	Regular Paper
Date Submitted by the Author:	n/a
Complete List of Authors:	De Vitis, Valerio; Universita degli Studi di Milano Dipartimento di Scienze per gli Alimenti la Nutrizione e l'Ambiente Nakhnoukh, Cristina; Università degli Studi di Milano, Dipartimento di Bioscienze Pinto, Andrea; Universita degli Studi di Milano Dipartimento di Scienze per gli Alimenti la Nutrizione e l'Ambiente Contente, Martina; Universita degli Studi di Milano Dipartimento di Scienze per gli Alimenti la Nutrizione e l'Ambiente; University of Nottingham School of Health Sciences, School of Chemistry Barbiroli, Alberto; Universita degli Studi di Milano Dipartimento di Scienze per gli Alimenti la Nutrizione e l'Ambiente Milani, Mario; Consiglio Nazionale delle Ricerche, Istituto di Biofisica Bolognesi, Martino; Università degli Studi di Milano, Dipartimento di Bioscienze; Università degli Studi di Milano; Consiglio Nazionale delle Ricerca , Istituto di Biofisica Molinari, Francesco; Universita degli Studi di Milano Dipartimento di Scienze per gli Alimenti la Nutrizione e l'Ambiente Gourlay, Louise; Università degli Studi di Milano, Dipartimento di Bioscienze Romano, Diego; Universita degli Studi di Milano Dipartimento di Scienze per gli Alimenti la Nutrizione e l'Ambiente
Key Words:	

Title: A stereospecific carboxyl esterase from *Bacillus coagulans* hosting non-lipase activity within a lipase-like fold

Valerio De Vitis[1], Cristina Nakhnoukh[2], Andrea Pinto[1], Martina Letizia Contente[1,3], Alberto Barbiroli[1], Mario Milani[4], Martino Bolognesi[2,4,5], Francesco Molinari[1], Louise J. Gourlay[2*] and Diego Romano[1*].

Affiliations:

[1] Department of Food, Environmental and Nutritional Sciences (DeFENS), Università degli Studi di Milano, Milano, Italy

[2] Department of Biosciences, Università degli Studi di Milano, Milano, Italy

[3] School of Chemistry, University of Nottingham, University Park, Nottingham, UK

[4] Biophysics Institute, National Research Council c/o Department of Biosciences, Università degli Studi di Milano, Via Celoria 26, 20133 Milano, Italy.

[5] Pediatric Research Center "Romeo e Enrica Invernizzi", Cryo Electron Microscopy Laboratory, University of Milano, Milano, Italy

[*] Joint corresponding authors

Correspondence:

Louise J. Gourlay, Department of Biosciences, Università degli Studi di Milano, Via Celoria 26, Milano, 20133, Italy

Fax: +39 02 50314895

Tel: +39 02 50314914

E-mail: louise.gourlay@unimi.it

Diego Romano, Department of Food, Environmental and Nutritional Sciences (DeFENS), Università degli Studi di Milano, Via Mangiagalli 25, Milan, Italy

Fax: +39 02 50319238

Tel: +39 02 50319134

E-mail: diego.romano@unimi.it

Running title: Structure-function studies of stereoselective BCE

Abbreviations: BCE, *Bacillus coagulans* carboxylesterase 1; CD, circular dichroism; EtOAc, ethyl

acetate; hMGL, human monoglyceride lipase; IPG, 1,2-*O*-isopropylidenglycerol; *p*NPA, *p*-nitrophenyl acetate.

Keywords: carboxylesterase; IPG; *Bacillus coagulans*; crystal structure; lipase, enantioselective.

Database: Coordinates and structure factors have been deposited in the Protein Data Bank (www.rcsb.org) under accession numbers 5O7G (apo-BCE) and 5OLU (glycerol-bound BCE).

Conflicts of Interest: The authors declare that there are no conflicts of interest.

Abstract

Microbial carboxylesterases are important biocatalysts that selectively hydrolyze an extensive range of chiral and prochiral esters. Here, we report the biochemical and structural characterization of an atypical carboxylesterase from *Bacillus coagulans* (BCE), endowed with high enantioselectivity towards different 1,2-*O*-isopropylideneglycerol (IPG or solketal) esters. BCE efficiently catalyzes the production of enantiopure (*S*)-IPG, a chiral building block for the synthesis of β-blockers, glycerophospholipids and prostaglandins; efficient hydrolysis was observed up to 65°C. To gain insight into the mechanistic bases of such enantioselectivity, we solved the crystal structures of BCE in apo- and glycerol-bound forms at resolutions of 1.9 Å and 1.8 Å, respectively. *In silico* docking studies on the BCE structure confirmed that IPG esters with small acyl chains (≤C6) were easily accommodated in the active site pocket, indicating that small conformational changes are necessary to accept longer substrates. Furthermore, docking studies suggested that enantioselectivity may be due to an improved stabilization of the tetrahedral reaction intermediate for the *S*-enantiomer. Contrary to the above functional data implying non-lipolytic functions, BCE displays a lipase-like 3D-structure that hosts a 'lid' domain capping the main entrance to the active site. In lipases the lid mediates catalysis through interfacial activation, a process that we did not observe for BCE. Overall, we present the functional-structural properties of an atypical carboxyl esterase that has non-lipase like functions, yet possesses a lipase-like 3D fold. Our data provide original enzymatic information in view of BCE applications as an inexpensive, efficient biocatalyst for the production of enantiopure *(S)*-IPG.

Introduction

Carboxylester hydrolases (EC 3.1.1.1) are enzymes that catalyze the cleavage or formation of carboxyl ester bonds, being often classified as esterases and lipases, based on experimental data and theoretical hypotheses. Recently, it has been suggested to simply organize carboxylester hydrolases into lipolytic esterases (proposed EC: L3.1.1.1) and non-lipolytic esterases (NLEst, proposed EC: NL3.1.1.1) [1]; however, they have also been classified, based on their sequence similarity and secondary structure conservation, taking advantage of databases, such as the Lipase Engineering Database (LED), the α/β-hydrolase Fold Enzyme Family 3DM or ESTHER [2, 3]. Lipolytic esterases and non-lipolytic esterases are useful biocatalysts, especially for the (stereo)selective hydrolysis or synthesis of chiral and prochiral esters, for the preparation of chiral drugs and their intermediates [4-6].

Bacteria belonging to the genus *Bacillus* are known producers of stereoselective carboxylesterases [7]. Lipolytic and non-lipolytic esterases from *B. subtilis* [8-13], *B. coagulans* [14], *B. amyloliquefaciens* [15], *B. stearothermophilus* [16], and generic *Bacillus* sp. [17] have been identified as excellent biocatalysts for the stereoselective hydrolysis of chiral and prochiral esters. This feature allows for the preparation of structurally different alcohols and carboxylic acids as single enantiomers.

Significant attention has been dedicated to the enantioselective hydrolysis of racemic esters of 1,2-*O*-isopropylideneglycerol (IPG or solketal) catalyzed by carboxylesterases, for the preparation of optically pure IPG [[8, 14, 18-23]. Enantiopure IPG is an inexpensive and valuable chiral building block for the synthesis of β-blockers, glycerophospholipids, and prostaglandins [24]. However, enantioselective hydrolysis of IPG esters is difficult to obtain with lipolytic esterases (lipases); in a systematic study using commercial lipases, the best result was found with Amano AK lipase (from *Pseudomonas* sp.), which hydrolyzed (*R,S*)-IPG octanoate with good enantioselectivity, but with low yields (22% after 48 h) [25]. Other lipases, including *Candida antartica* lipase B (Novozyme 435), were poorly enantioselective towards acetate and octanoate IPG [25].

We previously identified and purified a carboxylesterase from *B. coagulans* (BCE) with medium-to-high enantioselectivity towards different racemic esters [26], including esters of IPG [14, 23]. The attractive thermophilic and stereoselective properties led us to further investigate this enzyme from both a biochemical and structural point-of-view as a potential target for industrial applications. Here, we present the crystal structures of BCE, solved in its apo-form and in complex with glycerol, at 1.9 and 1.8 Å resolution, respectively. Moreover, we show that BCE functions as a

non-lipolytic carboxylesterase and hydrolyzes C2-C8 esters, with maximum activity towards caproate (C6) esters, and can catalyze the production of optically pure (*S*)-IPG from racemic mixtures of butyrate and benzoate IPG esters. BCE is active at reaction temperatures as high as 65°C, showing typical Michaelis-Menten kinetics and has no apparent requirement for interfacial activation. This latter observation, and such non-lipase-like functions, are in contrast with or structural results that highlight the presence of a particularly large, lipase-specific, lid domain that typically mediates interfacial activation in these enzymes. In view of the foreseen biotechnological applications, our structural and functional characterization of the lipase-like BCE is presented in relation to its non-lipolytic activity and of its stereoselectivity for butyrate and benzoate IPG esters.

Results

Production of recombinant BCE

The gene coding for BCE (accession number WP_029142894) was amplified from *B. coagulans* NCIMB 9365 genomic DNA and cloned into the pET100/D-TOPO® bacterial expression vector. N-terminal His-tagged BCE fusion protein was produced in *Escherichia coli* BL21(DE3)Star cells, as described in the Experimental Procedures. Expression levels were determined by SDS-PAGE (data not shown) and by measuring enzyme activity (U/mg), monitoring the conversion of *p*-nitrophenyl acetate (*p*NPA) to *p*-nitrophenol. The highest specific activity was measured after induction with 0.5 mM IPTG for 16 h at 20°C in Luria-Bertani (LB) broth.

BCE was purified by affinity chromatography and exchanged into 50 mM Tris-HCl pH 8.0, 100 mM NaCl for activity assays, as described in the Experimental Procedures. BCE migrated on a 11% polyacrylamide gel at a molecular weight of 40 kDa, consistent with the calculated molecular mass of the full-length protein (39.2 kDa) including the N-terminal His-tag (4.1 kDa). Under optimized conditions, 20 mU/mg of BCE was obtained, corresponding to a volumetric productivity of approximately 350 mU/L culture and to a specific productivity of 80 mU/g wet biomass.

BCE activity and enantioselectivity

BCE exhibited high activity towards *p*NPA between 45 and 65°C in 50 mM Tris-HCl pH 8.0 containing 100 mM NaCl; the highest activity was observed at 65°C. BCE was active at a pH range from 7.0 to 9.0.

The ability to hydrolyze substrates with longer acyl chains was investigated using *p*-nitrophenyl butyrate (C4), caproate (C6), caprylate (C8), caprate (C10), laurate (C12), and palmitate (C16) (**Figure 1**). BCE showed typical non-lipolytic behavior, being able to hydrolyze C2-C8 esters

following typical Michaelis-Menten kinetics, with a maximum activity towards caproate ester (see **Table 1** for kinetics data), whereas no activity was detected towards laurate and palmitate esters. The requirement for interfacial activation was also assessed by measuring the activity of BCE over a range (0.1-2.0 mM) of tributyrin concentrations (data not shown). Tributyrin is a short-chain triglyceride with low solubility in water that can form a lipid-water interface above the so-called saturation point. If interfacial activation occurs, a significant increase in substrate hydrolysis at the saturation point of tributyrin is expected, as observed with classical lipases [27]. Under all the experimental conditions tested, BCE did not display interfacial activation, confirming that it is not a lipase (data not shown).

The enantioselectivity of the purified recombinant BCE was assayed using three different IPG esters (acetate, butyrate, and benzoate; **Table 2**), previously tested with the native enzyme isolated directly from *B. coagulans* [14]. Hydrolysis of butyrate and benzoate esters occurred with high reaction rates and enantioselectivity (**Table 2**), whereas the biotransformation of the acetate ester was much slower and less enantioselective. Biotransformation of IPG benzoate was carried out also on a semi-preparative scale (200 mL), confirming the results obtained on smaller scale, and proving the applicability of recombinant BCE as a preparative biocatalyst.

The 3D structure of BCE

The 3D structures of ligand-free BCE and glycerol-bound BCE were solved using X-ray diffraction data collected on one single hexagonal (space group $P6_322$) crystal (per dataset) at resolutions of 1.9 Å and 1.8 Å, respectively, as described in the Experimental Procedures (**Figures 2A-C**). For both datasets, one BCE monomer was present in the asymmetric unit, with an estimated solvent content of 63.1% (Matthews coefficient of 3.3 $Å^3$/Da). Interestingly, the molecular replacement package BALBES revealed that the hexagonal BCE unit cell (a=138.1 Å, b=138.1 Å, c= 83.3 Å) is identical to that of a eukaryotic polyphosphate polymerase in complex with orthophosphate (PDB entry 3G3T); this is a coincidence since the two enzymes are completely unrelated. Both BCE structures were refined to satisfactory R_{free} and R_{gen} values (**Table 3**). Electron density was well-defined for almost all of the BCE polypeptide, except for the last C-terminal residue, and include an additional residue (in glycerol-bound BCE) or two (for ligand-free BCE) extra residues at the N-terminus that pertain to the cloning region of the pET100/D-TOPO bacterial expression vector.

Overall 3D Fold

Both BCE crystal structures are essentially identical (*rmsd* value 0.3 Å over the whole Cα backbone), displaying the canonical α/β hydrolase fold shared by all members of this superfamily.

The central β-sheet comprises seven parallel strands (β1 and β3-8) and one anti-parallel β-strand (β2) inserted between β-strands 1 and 3; eleven α-helices and two 3_{10} α-helices complete the whole structure (**Figure 2A**). In contrast to activity studies, which suggest that BCE is a non-lipolytic carboxylesterase, BCE presents a lipase-like 3D fold, deduced by the presence of an extra so-called 'lid domain', comprising three α-helices (α5, α6 and α8) that caps the entrance to the active site, housed in the canonical α/β hydrolase core (**Figure 2A**).

Accordingly, despite poor sequence conservation (25.1% sequence identity), the closest structural homolog (*rmsd* value of 1.72 Å over 154/304 Cα pairs) to BCE is human monoglyceride lipase (hMGL; PDB entry 3JWE [28]), as determined using Profunc (http://www.ebi.ac.uk/thornton-srv/databases/profunc/); structural conservation resides almost entirely in the α/β-hydrolase domain, while the lid domains differ significantly (**Figure 2C**). hMGL, like all mono- and diacylglycerol lipases studied to date, belongs to the single α-helix/loop lid lipase class [29]. If BCE were in fact a true lipase, it would pertain to the large-lid class characteristic of thermophilic lipases; however, in light of our activity data, it is likely that BCE belongs to an entirely different carboxyl esterase class altogether. Additional structural differences between the two proteins occur at the N-terminus; hMGL contains an extra α-helix, a shorter β-strand 1, and α2 in BCE is replaced by an unstructured loop in hMGL (**Figure 2C**).

The BCE lid domain

As mentioned above, the absence of interfacial activation for catalysis is contradictory to the presence of the lipase-specific lid-domain that would mediate this process. The BCE lid domain (residues 145-235) is particularly large, also with respect to the lids of the 21 other lipase members (of known structure) belonging to the large-lid lipase subclass [29]. Open and closed lid conformations have been crystallized for several lipases, however the BCE lid was found in the closed conformation in all datasets collected to date, despite the absence or presence of glycerol bound at the active site (**Figure 2B**). Only two lid residues (F209 and T210), housed in a 11-residue loop that connects α7 to α8 and forms the entrance to the active site, are diversely positioned. Interestingly in apo-BCE, the closed lid conformation does not completely block entrance to the active site, leaving an aperture with diameter of approximately 13 Å (**Figure 3A**). This aperture may permit the diffusion of small substrates directly into the active site without requiring lid repositioning. In the glycerol-bound enzyme, the repositioning of F209 and T210 is sufficient to partially close the active site aperture.

The presence of an active site aperture and the lack of classical lipolytic carboyxlesterase activity, however, do not rule out the possibility of lid switching between open and closed BCE

conformations during catalysis. Accordingly, molecular dynamics calculations were run using the online server PiSQRD (http://pisqrd.escience-lab.org) to assess BCE lid flexibility. MD simulations on glycerol-free BCE showed that the enzyme moiety consists of two main regions that behave as rigid units, moving independently from one another during protein structural fluctuations (under conditions of thermal equilibrium); region 1 comprises three stretches comprising residues 1-77, 86-142 and 228-309; region 2 comprises two stretches comprising residues 78-85 and 143-227. Regions 1 and 2 essentially match the core α/β-hydrolase domain and the lid domain, respectively, thus highlighting the potential dynamical role of the BCE lid [30].

The BCE active site

The BCE active site contains a conserved catalytic triad (S114, H284 and D251), with the catalytic S114 being housed in the conserved GXSXG (GSHMG in BCE) motif on β5, representing the nucleophilic elbow hosted in a turn that links β5 and α4. The oxyanion hole, which stabilizes the anionic transient tetrahedral catalytic intermediate, is built by the backbone NH groups of M115 and G116 in the nucleophilic elbow, and by residues G37 (Cα) and F38 (side-chain atoms). The active site-bound glycerol molecule, observed in several of the analyzed crystals, hydrogen-bonds with glycerol atom O2 and an interleaving water molecule (that also interacts with the hydroxyl group of S114) and, via glycerol atom O1 that bonds with adjacent residues H113(NE2), and E285(OE2) (**Figure 2C**).

Surface cavity analysis using CAST-P (www. http://sts.bioe.uic.edu/castp/) and the atomic coordinates of apo-BCE, revealed the solvent-accessible active site cavity (volume = 752 $Å^3$; area= 878 $Å^2$), which comprises main-chain and/or side chain atoms of 34 residues (**Figure 3A**) [31]. In glycerol-bound BCE, the size of this cavity increases (volume = 1028 $Å^3$; area= 1370 $Å^2$), however solvent accessibility decreases due to slight closure of the aperture to the active site as a result of repositioning of residues F209 and T210.

***In silico* docking of tested IPG ester substrates**

The BCE active site is accessible through a 13 Å wide tunnel that connects the catalytic triad to the solvent, branching into a side pocket next to the active residue S114 (**Figures 3A-B**); the terminal pocket is lined by hydrophobic residues mainly contributed by α-helix 6 (residues 167-178) of the lid. The pocket size is limited (maximal extension ~ 10 Å), making it unable to fit large aliphatic substituents. Analysis by *in silico* docking using the *p*-nitrophenyl synthetic substrates used in the activity experiments, shows that the active site can optimally accommodate 2-6 C atoms, with the best fit for a C6 aliphatic tail, in keeping with the observed enzymatic activity (**Figures 1 and 3B**).

Despite this size limitation, 90% activity was observed for *p*-nitrophenyl caprylate (C8), suggesting that conformational changes may occur (not evident by docking on a static structure), giving rise to a larger hydrophobic pocket (**Figure 1**). These changes are likely to occur in the lid due to its known flexible nature in lipases, and the contribution of its residues to shaping the hydrophobic pocket. Conformational changes however are likely to be contained, as demonstrated by the inability of BCE to hydrolyze > C10 substrates (**Figure 1**).

We next used *in silico* docking to explore the structural bases of BCE enantioselectivity. The dissociation constants (K_d) resulting from simulations on different IPG esters (acetate, butyrate, and benzoate) predicted different substrate affinities for BCE (K_d varying between 139 and 7.5 μM for the different compounds), but proved quite similar for the *R*- and *S*-enantiomers of each compound (**Table 4**). To further investigate this issue, the binding modes of three chiral IPG esters docked into the active site were analyzed, detecting fine structural differences that may shed light on the roots of the observed BCE enantioselectivity. In fact, a structural parameter that may promote enzymatic activity is the stabilization of the tetrahedral intermediate by H284 during the second step of the catalytic cycle [32]. Such stabilization is strictly related to the distance between the catalytic H284 NE atom and the O atom of the scissile ester bond. The simulations, run on the uncleaved substrate, show that (see **Table 4** and **Figure 3C**) such distance in IPG acetate is very similar in both the *R*- and *S*-enantiomers, in agreement with the BCE lower stereoselectivity levels *vs.* this substrate. On the contrary, the same distance is reduced from 5.0 Å, for the *R*-, to 4.3 Å for the *S*-enantiomer of the butyrate ester, respectively, suggesting that the tetrahedral intermediate originating from the *S*-enantiomer may be present as a more populated species during the catalytic cycle (**Figure 3C**). Although such considerations are only based on simulated enzyme:substrate models, and additional factors undoubtedly may hold, they suggest that BCE enantioselectivity should result from a combination of fine structural details, rather than from promptly identifiable substrate:active site recognition features.

Circular dichroism and thermal stability studies

The conformational stability of BCE in solution was characterized by circular dichroism (CD). In agreement with the crystal structure, the far-UV CD spectrum shows the typical features of α-helix rich proteins: two minima at 220 and 208 nm, and an intersection at zero at about 203 nm (**Figure 4, inset**). Thus, the thermal stability of BCE was assessed as a function of increasing temperature, monitoring the ellipticity at 220 nm (reporter of α-helix secondary structures), as described in the Experimental Procedures.

The BCE melting curve is biphasic, with a first minor conformational transition at 42°C (T_{m1}, 30% of the total transition) and a second main transition at 87°C (T_{m2}, 70% of the total transition) (**Figure 4A**). The second transition triggers a macroscopic aggregation of unfolded protein that causes irreversible denaturation. The reversibility of the first transition was studied by setting-up a multistep temperature ramp experiment. A BCE sample was heated in a first temperature ramp from 20 to 60°C and then cooled down to the starting temperature of 20°C. The same BCE sample was heated in a second temperature ramp up to 95°C (**Figure 4B**). In the second temperature ramp the first minor melting is no longer visible, whereas the second main transition is perfectly conserved, proving that the two transition are irreversible and, apparently, independent.

Although the structural regions involved in the first transition have not been identified, to gain better insight into the nature of these conformational transitions we carried-out activity assays on BCE, with and without heat-treatment. Interestingly, after 30 min at 60°C, also the heat-treated protein was catalytically competent, although a 90% decrease in activity was observed. According to the molecular dynamics calculations that divide the BCE structure into two distinct regions (the core α/β-hydrolase domain and the lid domain), we hypothesize that the lid domain may be responsible for the first unfolding event, affecting the catalytic function of BCE only marginally. This hypothesis is also in agreement with a "quantitative" analysis of the unfolding trace: the signal lost in the first transition is about 30% of the total, thus compatible with loss of the three α-helices of the lid relative to a total of the eleven α-helices of the whole structure. Lid unfolding would have a detrimental effect on binding of the hydrophobic tail of the substrate to BCE, whereas binding to the oxyanion hole would be essentially unaffected.

Protein thermostability can result from a number of structural features, such as the presence of disulfide bonds and intra-helical salt bridges [33]. BCE1 does not contain any disulfide bonds, and in fact, contains only one non-conserved cysteine residue (C137). Using the ESPRI web server (http://bioinformatica.isa.cnr.it/ESBRI/introduction.html), 21 salt bridges (2.4-3.9 Å) were mapped in BCE, none of which locates to the lid domain; nevertheless, two are formed between lid residue (D79) and residues R14(NZ) (3.2 Å) and R216(NH2) (3.1 Å (OD2) and 3.3 Å (OD1)) [33, 34]. These analyses also corroborate the theory that the α/β-hydrolase core is stable to a greater extent than the lid domain, supporting both the MD and CD studies, and reinforces the hypothesis that lid unfolding is responsible for the first unfolding transition.

Discussion

Carboxylesterases are ubiquitous enzymes that catalyze the cleavage and/or formation of carboxyl ester bonds. Their division into lipolytic (lipases) and non-lipolytic esterases is based on

experimental data and theoretical hypotheses; however, such classification is often quite uncertain. All carboxylesterases share the so-called α/β hydrolase fold, where five (or more) strands in a central β-sheet forming the protein core are connected by α-helices; this superfamily is one of the largest families of structurally related enzymes. Despite such elevated structural conservation, α/β-hydrolase members catalyze a wide variety of chemical transformations, and thus are extensively used in industrial processes. Lipases are characterized by the presence of a mobile smaller domain (lid), which caps and shields substrate entry to the active site. The closed-lid conformation is supposed to be preponderant in water, where most lipases are poorly active, whereas interactions with hydrophobic compounds (substrates, organic solvents) are thought to prompt a lid conformational change that promotes substrate accessibility to the active site (open-lid). Such overall phenomenon is generally referred as "interfacial activation" [35].

Due to their advantageous biochemical properties, such as high chemo-, regio- and stereo-selectivity, and thermostability, microbial carboxylesterases find numerous industrial applications in a wide range of sectors [4-6]. Kinetic resolution of racemic esters of chiral alcohols *via* their enantioselective hydrolysis is among the most studied application. Optically pure (*S*)-1,2-O-isopropylideneglycerol (IPG) is a key intermediate for the preparation of β-blockers, leukotrienes, phospholipids, and prostaglandins [24]. Hydrolysis of racemic IPG esters has been explored using different carboxylesterases aiming at optically pure (*S*)-IPG; however, commercially available lipases are generally poorly active or scarcely enantioselective towards racemic IPG esters [25]. We previously found that BCE, a carboxylesterase from *B. coagulans,* effectively carried out the kinetic resolution of different racemic IPG esters yielding (*S*)-IPG with high enantioselectivity [14]. Therefore, to gain insight into the structure-function properties of BCE that may account for such enantioselectivity for IPG esters, we carried out the recombinant production, functional characterization and 3D structure analyses of BCE (ligand-free and glycerol-bound).

Recombinant BCE, here presented, successfully catalyzed the enantioselective hydrolysis of different IPG esters, providing optically pure *(S)*-IPG with good reaction rates and excellent enantiomeric ratios; the best results being obtained with butyrate (C4) and benzoate (C6) IPG ester substrates. The enzymatic activity, however, dropped by 10% for C8 chains, by 90% for C10 substrate aliphatic chains, and was completely abolished for C12 and C16 chains. The BCE crystal structure shows that substrates with aliphatic tail lengths shorter or equal to C6 can snugly be docked into the active site hydrophobic pocket. This is contradictory to the high activity observed with C8 *p*-nitrophenyl substrates, suggesting that a conformational change, or dynamic adaptation, must occur to accommodate these extra atoms. We propose that these changes mostly affect the lid

domain, due to the role of hydrophobic lid residues (in α-helix 6) in binding the aliphatic carbon tail of the substrate, and to its proposed dynamic nature.

CD thermal stability ramps show two unfolding events, identified by T_M values of 42°C and 87°C, respectively. We hypothesize that the first event reflects the unfolding of the lid domain, as indicated by MD studies and structural observations that underline the presence of 21 stabilizing salt bridges in the α/β-hydrolase core, while none would stabilize the lid domain.

Poor activity towards long-chain esters, together with IPG ester enantioselectivity are typical features of non-lipolytic carboxylesterases. Moreover, benzoate esters, the preferred substrate of BCE, are not preferred substrates for lipases (with the exception of the very versatile *Candida antartica* Lipase B-CALB) [36]. Such functional findings are in sharp contrast with what would be suggested by the BCE 3D-structure that highlights the presence of a lipase-typical lid domain, in addition to the canonical α/β-hydrolase fold. Considering the role played by the lid domain in the interfacial activation process, where optimal reaction rates are observed at the hydrophobic-water interface, we carried out experiments in the presence of a triglyceride layer produced by the addition of tributyrin. In agreement with our activity studies, but in contrast with the presence of the lipase-specific lid domain, interfacial activation was not observed. The lack of interfacial activation, and the fact that BCE was able to convert the (small) substrates used in this study in water with conventional kinetics, was also implied by the absence of lid re-positioning in the ligand-free and in the glycerol-bound structures. Interestingly, despite the observed 'closed' lid state of ligand-free BCE, access to the substrate-binding site was not completely blocked since a 13 Å mouth-opening to the active site tunnel was observed that could easily permit diffusion of IPG esters to the catalytic center. Despite the non-lipase functions here reported, we cannot rule out switching of the lid domain between 'open' and 'closed' conformations; in fact, *in silico* simulations carried out on the BCE 3D structure, focusing on protein flexibility and rigid body movements, identified the lid domain as a potentially mobile entity.

Our studies reveal that BCE is an atypical carboxylesterase characterized by non-lipolytic functionalities, while hosting a lipase-like 3D fold. With regards to the enantioselective hydrolysis of short-chain and benzoate esters of IPG, with a preference for *(S)*-IPG esters, *in silico* docking studies suggest that a reduced distance between the catalytic histidine residue (H284 that stabilizes the tetrahedral reaction intermediate during catalysis) and the ester O atom of the substrate, may play a selection role. Thanks to the here-reported crystal structures, *in silico* docking may be used to search for inhibitors that may be used in co-crystallization studies to reveal all the active site components that govern such specificity. Our results may pave the way for rational engineering strategies aimed at the construction of new BCE variants with wider substrate specificities, and thus

suited for different applications as stereoselective biocatalysts

Experimental Procedures

Production of recombinant BCE

The BCE gene coding for the full-length protein was amplified from *B. coagulans* genomic strain NCIMB 9365 DNA by PCR using the following primers: Forward: 5'-CACCATGTTGGCTTTTCAAGAGTTGAG-3'; Reverse: 5'-TGAGCTCGAGTCATTTTACGATGATCCCGTT-3'. The amplified gene was cloned into the pET100/D-TOPO® vector (Invitrogen) in frame with a N-terminal six-histidine tag, according to the manufacturer's instructions. Correct construct sequence was confirmed by DNA sequencing.

Cultures of BL21(DE3)Star *E. coli* cells were transformed with the resulting plasmid and grown overnight at 37 °C in LB medium supplemented with 100 mg/L ampicillin. The seed culture was then diluted into 1.0 L Erlenmeyer flasks containing 100 ml Luria Broth (LB) at an initial OD_{600nm} of 0.1. Cultivation was carried out at 37 °C with agitation at 150 rpm. Cells were grown until an OD_{600nm} of 0.8. After cold-shock treatment, cultures were induced with 0.5 mM IPTG (isopropyl- β-D-thiogalactopyranoside) and further incubated for 16 h at 20 °C. Bacterial cells were harvested by centrifugation at 5000 rpm for 15 min, washed once with 20 mM sodium phosphate buffer at pH 7.0 and stored at -20 °C.

The cell pellet was resuspended in 50 mM Tris-HCl pH 8.0 containing 100 mM NaCl, 6 mM imidazole. Bacterial cells were lysed by sonication (5 cycles of 30 s each, in ice, with 1 min interval) and the supernatant was harvested by centrifugation at 15,000 rpm for 45 min at 4 °C. BCE was purified from the supernatant by affinity chromatography with HIS-Select Nickel Affinity Gel (Sigma-aldrich) pre-equilibrated with 50 mM Tris-HCl pH 8.0, containing 100 mM NaCl, 6 mM imidazole. After a washing step with 50 mM Tris-HCl pH 8.0, 100 mM NaCl, 6 mM imidazole, His-BCE was eluted with 50 mM Tris-HCl pH 8.0, 100 mM NaCl, 250 mM imidazole.

For crystallization trials, BCE was purified from a 0.5L bacterial culture on a 5 ml Bio-scale Mini Profinity IMAC cartridge using the Profinia Protein Purification System (Bio-rad), following standard Bio-rad protocols. Purified BCE was exchanged into crystallization buffer (10 mM Tris-HCl pH 8.0; 150 mM NaCl) using a PD10 desalting column (GE Healthcare), according to the manufacturer's instructions and concentrated to 6.5 mg/ml, using an Amicon Ultra-15 centrifugal filter (Millipore) with a MW cut-off of 10 kDa.

Biotransformations of IPG esters

Biotransformations of IPG esters were carried out in 5 mL screw capped tube, using 7 mU of BCE in 1 mL of 50 mM Tris-HCl pH 8.0, 100 mM NaCl. The substrates were added at the final concentration of 5 mM, dissolved in DMSO at a final concentration of 0.5%. Incubations were carried out with magnetic stirring at 30°C. Conversions and stereochemical outcomes were monitored by gas chromatography using a chiral capillary column (diameter 0.25 mm, length 25 m, thickness 0.25 µm, DMePeBeta-CDX-PS086, MEGA, Legnano, Italy) with a 0.25 mm-diameter, 25 m-length and 0.25 m-thickness, using the following temperature gradients: for IPG acetate: 10 min at 90 °C, increased to 120 °C over 15 min, maintained at 120 °C for 10 min and then increased to 180 °C over 2 min and then maintained at 180 for 10 min; for IPG butyrate: 10 min at 90 °C, increased to 110 °C over 5 min, maintained at 110 °C for 10 min and then increased to 180 °C over 2 min and then maintained at 180 for 10 min; for IPG benzoate: 10 min at 90 °C, increased to 120 °C over 3 min, maintained at 120 °C for 10 min and then increased to 180 °C over 2 min and then maintained at 180 for 10 min. Retention times of IPG enantiomers and esters under these conditions were: (*R*)-IPG= 8.2 min, (*S*)-IPG= 9.0 min; (*R*)-IPG acetate = 13.1 min, (*S*)-IPG acetate = 12.4 min; (*R*)-IPG butyrate =22.3 min, (*S*)-IPG butyrate = 21.2 min; (*R*)-IPG benzoate = 27.7 min, (*S*)-IPG benzoate = 27.5 min. Enantiomeric excesses (e.e.) were calculated using the following formulas: $e.e._{substrate}$ = ([(*S*)-IPG ester] - [(*R*)-IPG ester])/ ([(*S*)-IPG ester] + [(*R*)-IPG ester]) and $e.e._{product}$ = ([(*S*)-IPG] - [(*R*)-IPG])/ ([(*S*)-IPG] + [(*R*)-IPG])

Hydrolysis of IPG benzoate was also performed on semi-preparative scale: 250 mg (1.06 mmol) of substrate were dissolved in DMSO (1 mL) and added to 199 mL of 50 mM Tris-HCl pH 8.0, containing 100 mM NaCl. Upon addition of BCE (7 mU mL^{-1}), the reaction was followed by gas-chromatography and stopped after 50 min (in correspondence to a 60% conversion). The reaction was stopped by adding 100 mL ethyl acetate (EtOAc) to recover both unreacted (*S*)-IPG benzoate and enantiomerically pure (*S*)-IPG. The aqueous phase was extracted by repeating the addition of EtOAc twice. Organic extracts were collected, dried over sodium sulfate and the solvent removed under reduced pressure. Flash chromatography (*n*-hexane/EtOAc, 75/25) on silica gel pretreated with triethylamine afforded 52 mg of optically pure (*S*)-IPG (ee > 99% by chiral GC).

Activity and kinetic analyses of BCE activity

Kinetic parameters were measured spectrophotometrically using different concentrations of *p*-nitrophenyl esters (actetate, butyrate, caproate, caprylate, laurate, and palmitate) at 28°C in 1 mL of 50 mM Tris-HCl pH 8.0, 100 mM NaCl (final acetone concentration of 0.3%), monitoring the increase in absorbance at 400 nm due to the production of *p*-nitrophenol (15000 $M^{-1}cm^{-1}$). Experimental data were fitted to suitable kinetic models with Origin 9.0 and kinetic parameters

(V_{max}, K_M) were calculated using the same program. BCE activity (0.036 mg mL^{-1}) was routinely measured spectrophotometrically using 0.015 mM *p*-NPA as a substrate, following the reaction for 5 min. One unit of BCE corresponds to the amount of protein that produces 1 μmol of *p*-nitrophenol in 1 min. Tributyrin hydrolysis was measured titrimetrically over a range of tributyrin concentrations (0.1-2.0 mM) at 37 °C with a pH-stat, using 30 mL 10 mM phosphate buffer pH 7.0 [27].

BCE crystallization

Crystallization trials of BCE (6.5 mg/ml) were prepared in 96-flat well sitting drop plates (Greiner), containing 100 μL crystallization solution of PACT Premier™ Crystallization screen (Molecular Dimensions). 400 nL drops were deposited at diverse protein concentrations (30, 50 and 70 % of the stock protein solution) and crystals grew after approximately 1 week in several conditions. Data for the apo-enzyme were collected on a single crystal grown in condition 2-11 (20% PEG3350; 0.1 M sodium citrate tribasic hydrate); the crystal was cryoprotected in 50% PEG3350. Data for the glycerol-bound form of BCE were collected on a single crystal grown in condition 42 (1.5 M ammonium sulfate, 12% glycerol and 0.1 M Tris-HCl, pH 8.0) of Hampton Crystal Screen II (Hampton Research). For cryoprotection the concentration of glycerol was raised to 25%.

Data Collection, model building and refinement

X-ray diffraction Data were collected at the ID29 (glycerol-bound enzyme), ID23-1 (apo-enzyme) beamlines at the European Synchrotron Radiation Facility (ESRF, Grenoble, France). Data were processed using XDS and assigned to the hexagonal $P6_322$ space group using POINTLESS and scaled using AIMLESS, available in the CCP4i suite [37-39]. The 3D structure of BCE was solved *via* molecular replacement using BALBES and the protein sequence as the input; the BALBES search model was based on the structure of human monoglyceride lipase (PDB entry 3PE6) [40, 41]. The initial model was refined with PHENIX.refine, including a translational-libration-screw (TLS) option; final R_{gen} and R_{free} values of 21 and 24.3% (apo-BCE) and 14.7 and 16.9% (glycerol-bound BCE) were reached, respectively (**Table 3**). Both final models present ideal geometric parameters, with 97.7% (apo-BCE) and 98.1% (glycerol-bound BCE) residues assigned to the most favorable regions of the Ramachandran plot, with no outliers, according to structure validation using MolProbity under the Phenix platform (**Table 3**).

Circular dichroism

CD measurements were performed with a J-810 spectropolarimeter (JASCO Corp., Tokyo, Japan) equipped with a Peltier system for temperature control. All measurements were performed in crystallization buffer (10 mM Tris-HCl pH 8, 150 mM NaCl) at a protein concentration of 0.2 mg/ml, and in a 0.1 cm path length cuvette. Temperature ramps experiments were monitored at a wavelength of 220 nm (temperature slope 1°C/min). T_ms were calculated as the maximum of the first-derivative of the traces.

Acknowledgements

LJG and DR gratefully acknowledge departmental Università degli Studi di Milano 'Linea 2' funding.

Author contributions

VdV and DR designed and performed the experiments involving the preparation and purification of the recombinant enzymes. AP and MLC synthesized all substrates and optimized the analytical conditions. VdV and DR performed all the experiments of enzyme characterization and biotransformations. FM and MB analyzed the data, and wrote the manuscript. AB performed the CD experiments and wrote the manuscript. CN and LJG carried out purification, crystallization and 3D structure analyses. MM carried out *in silico* docking, related structural analyses and wrote the related section. DR and LJG coordinated the work and wrote the manuscript.

References

1. Ali, Y. B., Verger, R. & Abousalham, A. (2012) Lipases or esterases: does it really matter? Toward a new bio-physico-chemical classification, *Methods in molecular biology.* **861**, 31-51.

2. Hotelier, T., Renault, L., Cousin, X., Negre, V., Marchot, P. & Chatonnet, A. (2004) ESTHER, the database of the alpha/beta-hydrolase fold superfamily of proteins, *Nucleic acids research.* **32**, D145-7.

3. Kourist, R., Jochens, H., Bartsch, S., Kuipers, R., Padhi, S. K., Gall, M., Bottcher, D., Joosten, H. J. & Bornscheuer, U. T. (2010) The alpha/beta-hydrolase fold 3DM database (ABHDB) as a tool for protein engineering, *Chembiochem : a European journal of chemical biology.* **11**, 1635-43.

4. Carvalho, A. C., Fonseca Tde, S., de Mattos, M. C., de Oliveira Mda, C., de Lemos, T. L., Molinari, F., Romano, D. & Serra, I. (2015) Recent Advances in Lipase-Mediated Preparation of Pharmaceuticals and Their Intermediates, *International journal of molecular sciences.* **16**, 29682-716.

5. Romano, D., Bonomi, F., de Mattos, M. C., de Sousa Fonseca, T., de Oliveira Mda, C. & Molinari, F. (2015) Esterases as stereoselective biocatalysts, *Biotechnology advances.* **33**, 547-65.

6. Gotor-Fernandez, V., Brieva, R and Gotor, V (2006) Lipases: Useful biocatalysts for the preparation of pharmaceuticals., *J Mol Catal.* **40**, 111-120.

7. Guncheva, M., Zhiryakova, D. (2011) Catalytic properties and potential applications of Bacillus lipases., *J Mol Catal.* **B68**, 1-21.

8. Droge, M. J., Bos, R. & Quax, W. J. (2001) Paralogous gene analysis reveals a highly enantioselective 1,2-O-isopropylideneglycerol caprylate esterase of Bacillus subtilis, *European journal of biochemistry.* **268**, 3332-8.

9. Quax, W. J. & Broekhuizen, C. P. (1994) Development of a new Bacillus carboxyl esterase for use in the resolution of chiral drugs, *Applied microbiology and biotechnology.* **41**, 425-31.

10. Rozeboom, H. J., Godinho, L. F., Nardini, M., Quax, W. J. & Dijkstra, B. W. (2014) Crystal structures of two Bacillus carboxylesterases with different enantioselectivities, *Biochimica et biophysica acta.* **1844**, 567-75.

11. Schmidt, M., Henke, E., Heinze, B., Kourist, R., Hidalgo, A. & Bornscheuer, U. T. (2007) A versatile esterase from Bacillus subtilis: cloning, expression, characterization, and its application in biocatalysis, *Biotechnology journal.* **2**, 249-53.

12. Steenkamp, L., Brady, D. (2008) Optimisation of stabilised carboxylesterase NP for enantioselective ester hydrolysis of naproxen methyl ester., *Process Biochem.* **43**, 1419-26.

13. van Pouderoyen, G., Eggert, T., Jaeger, K. E. & Dijkstra, B. W. (2001) The crystal structure of Bacillus subtilis lipase: a minimal alpha/beta hydrolase fold enzyme, *Journal of molecular biology.* **309**, 215-26.

14. Molinari, F., Brenna, O., Valenti, M., Aragozzini, F. (1996) Isolation of a novel carboxylesterase from Bacillus coagulans with high enantioselectivity toward racemic esters of 1,2-O-isopropylideneglycerol., *Enzyme Microb Technol.* **19**, 551-6.

15. Liu, J. Y., Zheng G.W., Imanaka, T, Xu J.H. (2014) Stepwise and combinatorial optimization of enantioselectivity for the asymmetric hydrolysis of 1-(3',4'-methylenedioxyphenyl)ethyl acetate under use of a cold-adapted Bacillus amyloliquefaciens esterase, *Biotechnol Bioprocess Eng.* **99**, 442-8.

16. Henke, E. & Bornscheuer, U. T. (2002) Esterases from Bacillus subtilis and B. stearothermophilus share high sequence homology but differ substantially in their properties, *Applied microbiology and biotechnology.* **60**, 320-6.

17. Fillat, A., Romea, P., Urpi, F., Pastor, F. I. & Diaz, P. (2014) Improving enantioselectivity towards tertiary alcohols using mutants of Bacillus sp. BP-7 esterase EstBP7 holding a rare GGG(X)-oxyanion hole, *Applied microbiology and biotechnology.* **98**, 4479-90.

18. Godinho, L. F., Reis, C.R., van Merkerk R., Poelarends G-L., Quax W.J. (2012) An esterase with superior activity and enantioselectivity towards 1,2-O-isopropylideneglycerol esters obtained by protein design., *Adv Synth Catal.* **354**, 3009-15.

19. Godinho, L. F., Reis, C. R., Rozeboom, H. J., Dekker, F. J., Dijkstra, B. W., Poelarends, G. J. & Quax, W. J. (2012) Enhancement of the enantioselectivity of carboxylesterase A by structure-based mutagenesis, *Journal of biotechnology.* **158**, 36-43.

20. Godinho, L. F., Reis, C. R., Tepper, P. G., Poelarends, G. J. & Quax, W. J. (2011) Discovery of an Escherichia coli esterase with high activity and enantioselectivity toward 1,2-O-isopropylideneglycerol esters, *Applied and environmental microbiology.* **77**, 6094-9.

21. Molinari, F., Romano, D., Gandolfi, R., Kroppenstedt, R. M. & Marinelli, F. (2005) Newly isolated Streptomyces spp. as enantioselective biocatalysts: hydrolysis of 1,2-O-isopropylidene glycerol racemic esters, *Journal of applied microbiology.* **99**, 960-7.

22. Monti, D., Ferrandi, E. E., Righi, M., Romano, D. & Molinari, F. (2008) Purification and characterization of the enantioselective esterase from Kluyveromyces marxianus CBS 1553, *Journal of biotechnology.* **133**, 65-72.

23. Romano, D., Falcioni, F, Mora, D. and Molinari, F. (2005) Enhanced enantioselectivity of Bacillus coagulans in the hydrolysis of 1,2-O-isopropylidene glycerol esters by thermal knock-out of undesired enzymes, *Tetrahedron Asymmetry.* **16**, 841-5.

24. Jurczac, J., Pikul, S., Bauer, T., (1986) *Tetrahedron Asymmetry.* **42**, 447-488.

25. Machado, A., da Silva, A., Borges, C., Simas, A, Freire, D. (2011) Kinetic resolution of (R,S)-1,2-isopropylidene glycerol (solketal) ester derivatives by lipases, *Journal of Molecular Catalysis B: Enzymatic* **69**, 42-46.

26. Romano, A., Romano, D, Molinari, F, Gandolfi, R & Costantino, F (2005) A new chemoenzymatic synthesis of D-cloprostenol. , *Tetrahedron: Asymmetry* **16**, 3279-3282.

27. Thirstrup, K., Verger, R. & Carriere, F. (1994) Evidence for a pancreatic lipase subfamily with new kinetic properties, *Biochemistry.* **33**, 2748-56.

28. Bertrand, T., Auge, F., Houtmann, J., Rak, A., Vallee, F., Mikol, V., Berne, P. F., Michot, N., Cheuret, D., Hoornaert, C. & Mathieu, M. (2010) Structural basis for human monoglyceride lipase inhibition, *Journal of molecular biology.* **396**, 663-73.

29. Khan, F. I., Lan, D., Durrani, R., Huan, W., Zhao, Z. & Wang, Y. (2017) The Lid Domain in Lipases: Structural and Functional Determinant of Enzymatic Properties, *Frontiers in bioengineering and biotechnology.* **5**, 16.

30. Aleksiev, T., Potestio, R., Pontiggia, F., Cozzini, S. & Micheletti, C. (2009) PiSQRD: a web server for decomposing proteins into quasi-rigid dynamical domains, *Bioinformatics.* **25**, 2743-4.

31. Dundas, J., Ouyang, Z., Tseng, J., Binkowski, A., Turpaz, Y. & Liang, J. (2006) CASTp: computed atlas of surface topography of proteins with structural and topographical mapping of functionally annotated residues, *Nucleic acids research.* **34**, W116-8.

32. Hosokawa, M. (2008) Structure and catalytic properties of carboxylesterase isozymes involved in metabolic activation of prodrugs, *Molecules.* **13**, 412-31.

33. Kumar, S., Tsai, C. J., Ma, B. & Nussinov, R. (2000) Contribution of salt bridges toward protein thermostability, *Journal of biomolecular structure & dynamics.* **17 Suppl 1**, 79-85.

34. Kumar, S. & Nussinov, R. (1999) Salt bridge stability in monomeric proteins, *Journal of molecular biology.* **293**, 1241-55.

35. Reis, P. H., K. Watzke, H. Leser. ME and Miller ,R. (2009) Lipases at interfaces: a review., *Adv Colloid Interface Sci* **147–148**, 237–250.

36. Sangeeta, N. A., B. Rakhi, S. Bhawna, M. Pritish, P. Robin, C. Jesper, B. and Allan, S. (2010) Lipases for use in industrial biocatalysis: Specificity of selected structural groups of lipases, *Journal of Molecular Catalysis B: Enzymatic.* **65**.

37. Evans, P. (2006) Scaling and assessment of data quality, *Acta crystallographica Section D, Biological crystallography.* **62**, 72-82.

38. Kabsch, W. (2010) Xds, *Acta crystallographica Section D, Biological crystallography.* **66**, 125-32.

39. Kabsch, W. (2010) Integration, scaling, space-group assignment and post-refinement, *Acta crystallographica Section D, Biological crystallography.* **66**, 133-44.

40. Long, F., Vagin, A. A., Young, P. & Murshudov, G. N. (2008) BALBES: a molecular-replacement pipeline, *Acta crystallographica Section D, Biological crystallography.* **64**, 125-32.

41. Schalk-Hihi, C., Schubert, C., Alexander, R., Bayoumy, S., Clemente, J. C., Deckman, I., DesJarlais, R. L., Dzordzorme, K. C., Flores, C. M., Grasberger, B., Kranz, J. K., Lewandowski, F., Liu, L., Ma, H., Maguire, D., Macielag, M. J., McDonnell, M. E., Mezzasalma Haarlander, T., Miller, R., Milligan, C., Reynolds, C. & Kuo, L. C. (2011) Crystal structure of a soluble form of human monoglyceride lipase in complex with an inhibitor at 1.35 A resolution, *Protein science : a publication of the Protein Society.* **20**, 670-83.

42. Morris, G. M., Huey, R., Lindstrom, W., Sanner, M. F., Belew, R. K., Goodsell, D. S. & Olson, A. J. (2009) AutoDock4 and AutoDockTools4: Automated docking with selective receptor flexibility, *Journal of computational chemistry.* **30**, 2785-91.

43. Pettersen, E. F., Goddard, T.D., Huang, C.C., Couch, G.S., Greenblatt, D.M., Meng, E.C., Ferrin, T.E. (2004) UCSF Chimera--a visualization system for exploratory research and analysis. , *J Comput Chem.* **25**, 1065-12.

Tables

Table 1. Kinetic parameters for the hydrolysis of *p*-nitrophenyl esters catalyzed by BCE. Kinetic data were measured spectrophotometrically using different concentrations of *p*-nitrophenyl esters at 28°C in 50 mM Tris-HCl pH 8.0 containing 100 mM NaCl and acetone (final concentration 0.3%).

Substrate	k_{cat} (s^{-1})	K_M (mM)
acetate (C2)	0.621 (± 0.095)	0.873 (± 0.010)
butyrate (C4)	0.264 (± 0.025)	0.049 (± 0.006)
caproate (C6)	0.211 (± 0.020)	0.021 (± 0.005)
caprylate (C8)	0.105 (± 0.004)	0.003 (± 0.001)

Table 2. Hydrolysis of IPG derivatives by BCE. Conditions: 5 mM substrates, 7 mU/mL BCE in 50 mM Tris-HCl pH 8.0 containing 100 mM NaCl, and 0.5% *(v/v)* DMSO. Reactions were monitored by chiral gas chromatography (GC).

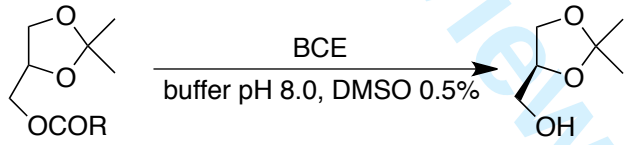

R	Conversion (%)	e.e.$_{substrate}$ (%)	e.e.$_{product}$ (%)	E[a]	Time (h)
CH_3	46	79 (*S*)	93 (*S*)	67	24
$(CH_2)_2CH_3$	42	70 (*S*)	97 (*S*)	139	1
Ph	49	92 (*S*)	96 (*S*)	163	0.5

[a] E refers to enantiomeric ratio

Table 3. **Data collection, refinement and validation parameters.** Data are shown for the two BCE datasets. [a]$R_{merge} = \sum |I-\langle I \rangle| / \sum I \times 100$, where I is the intensity of a reflection and $\langle I \rangle$ is the average intensity; [b]$R_{gen} = \sum |F_o-F_c| / \sum |F_o| \times 100$; [c]$R_{free}$ was calculated from 5% of randomly selected data for cross-validation. Values in parentheses represent data belonging to highest resolution shells (Apo-BCE; 1.9-1.94 Å; glycerol-bound BCE 1.8-1.84 Å).

	apo-BCE	BCE+glycerol
Data collection		
Space group	$P6_322$	$P6_322$
Cell dimensions		
a, *b*, *c* (Å)	138.6 138.6 83.8	137.6 137.6 83.6
α,β,γ (°)	90, 90, 120	90, 90, 120
Resolution (Å)	40-1.9	40-1.8
[a]R_{merge}	0.087 (0.504)	0.113 (0.598)
$I/\sigma I$	26.8 (7.8)	34.9 (8.9)
No. unique reflections	37667 (2359)	43646 (2545)
Completeness (%)	99.8 (99.5)	99.9 (99.8)
Redundancy	19.4 (20.4)	39.1 (37.6)
Refinement		
Resolution (Å)	40-1.9	40-1.8
[b]R_{gen} / [c]R_{free}	21.6/24.3	14.7/16.9
No. atoms:		
Protein	2456	4807
Glycerol	-	18
Chloride ion	-	8
Acetate ion	-	4
Polyethylene glycol	-	6
Water	50	192
B-factors (Å^2):		
Protein	23.9	21.9
Glycerol	-	27.5
Chloride ion	-	44.0
Acetate ion	-	38.7
polyethylene glycol	-	56.2
Water	30	24.1
R.m.s. deviations:		
Bond lengths (Å)	0.014	0.007
Bond angles (°)	1.258	0.856
Ramachandran Plot (%)		
Favored Regions	97.7	98.1
Allowed Regions	100	100

Table 4. *In silico* docking of -acetate, -butyrate and -benzoate IPG esters to the active site of BCE. The calculated dissociation constants (K_d) for the S- and R-enantiomers of the -acetate, -butyrate and -benzoate IPG esters are reported together with the distances between H284 NE atom and the substrate ester O atom. Docking was carried out using Autodock 4.2 [42].

Compound	(R) K_d [μM]	(S) K_d [μM]	dist. O-H284 (R) (Å)	dist. O-H284 (S) (Å)
Acetate-IPG	139.2	137.6	5.0	5.0
Butyrate-IPG	41.9	43	5.0	4.3
Benzoate-IPG	9.9	7.5	5.7	5.4

Figure Legends

Figure 1. BCE activity towards *p*-nitrophenyl esters. Relative activity refers to the activity in the presence of *p*-nitrophenyl caproate (100%), and represents the arithmetic mean and standard deviation (SD) of three measurements.

Figure 2. The crystal structure of apo-BCE and structural comparisons with hMGL. (A) Ribbon secondary structure representation of the crystal structure of apo-BCE. α-helices (blue) and β-strands (grey) and the N- and C-termini are labeled. The lid domain comprising α-helices 5, 6 and 8 is indicated. (B) View of the interaction between glycerol and BCE residues H113, E284 and a conserved water molecule (W27); hydrogen bonds are indicated by dotted lines. Interaction residues and catalytic triad (S114, H284, D251) residues are labeled and shown as sticks. (C) Superposition of the crystal structures of apo-BCE (blue) and inhibitor-bound hMGL (grey; PDB entry 3JWE,

[28]). Structural variations are highlighted in shading. All figures were generated using Chimera [43].

Figure 3. Analysis of the BCE substrate-binding site. A) Detailed view of the apo-BCE active site, highlighting the active site tunnel (surface representation); the entrance to the tunnel and the hydrophobic region of the active site are indicated. Hydrophobic residues, the catalytic S114 and the R- and S- enantiomers of butyrate-IPG (sticks) that were *in silico* docked to the active site are shown; B) *in silico* docking of *p*-nitrophenyl compounds (sticks) with different acyl chains of variable lengths; C2 (pink), C4 (ochre) and C6 (purple); **C)** Illustration of the bond distances between the substrate ester O atom and H284 NE atom in R- (yellow) and S-(blue) butyrate-IPG. Docking was carried out using Autodock4.2 [42].

Figure 4. Conformational stability of BCE. (A) Thermal unfolding of BCE monitored through far-UV CD at 220 nm, as described in the Experimental procedures. The two transitions are labeled T_{m1} and T_{m2}, respectively. Inset: BCE far-UV CD spectrum; (B) the reversibility of the first conformational transition was evaluated by thermal unfolding of BCE, monitored through far-UV CD at 220 nm at protein concentration of 0.1 mg/mL. BCE was heated from 20°C to 60°C (blue line) and then cooled down to 20°C The same sample was heated up to 95°C (red line). The two transitions are labeled T_{m1} and T_{m2}, respectively. In this experiment, T_{m2} occurs at higher temperature due to the lower protein concentration.

Figure 1

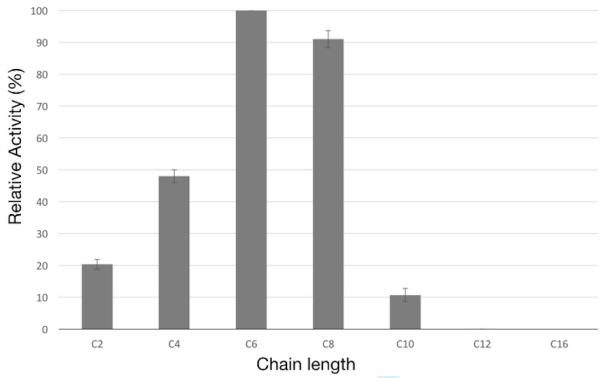

Figure 2

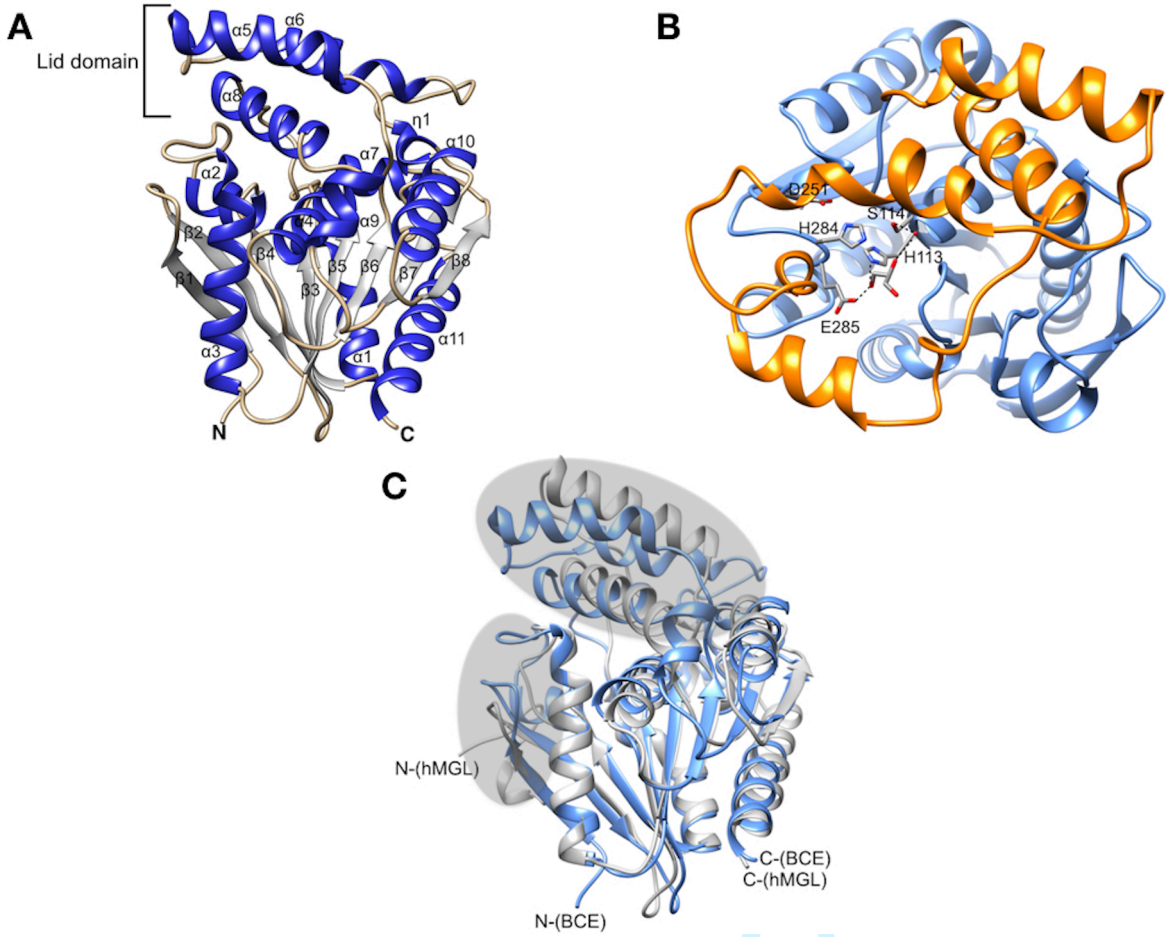

Figure 3

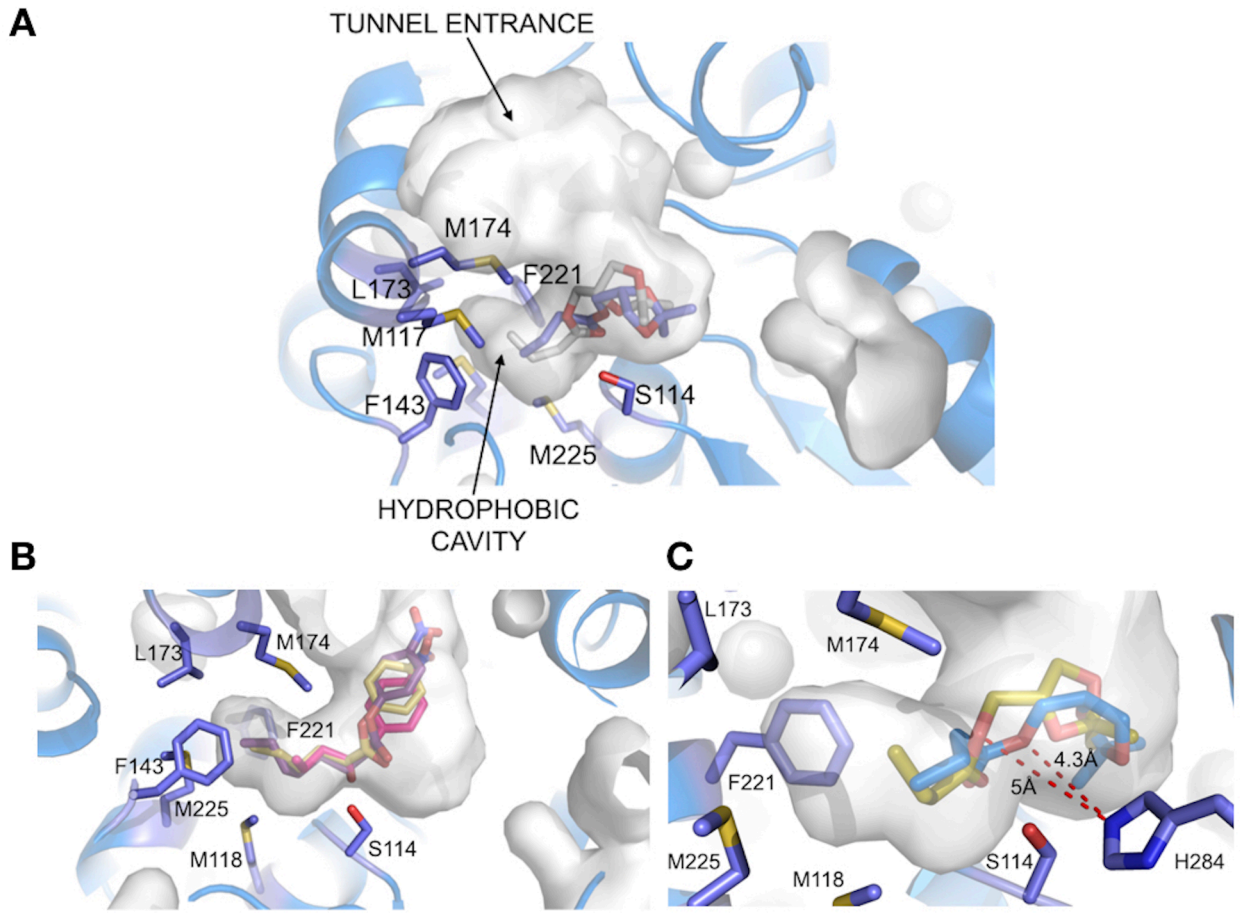

Figure 4

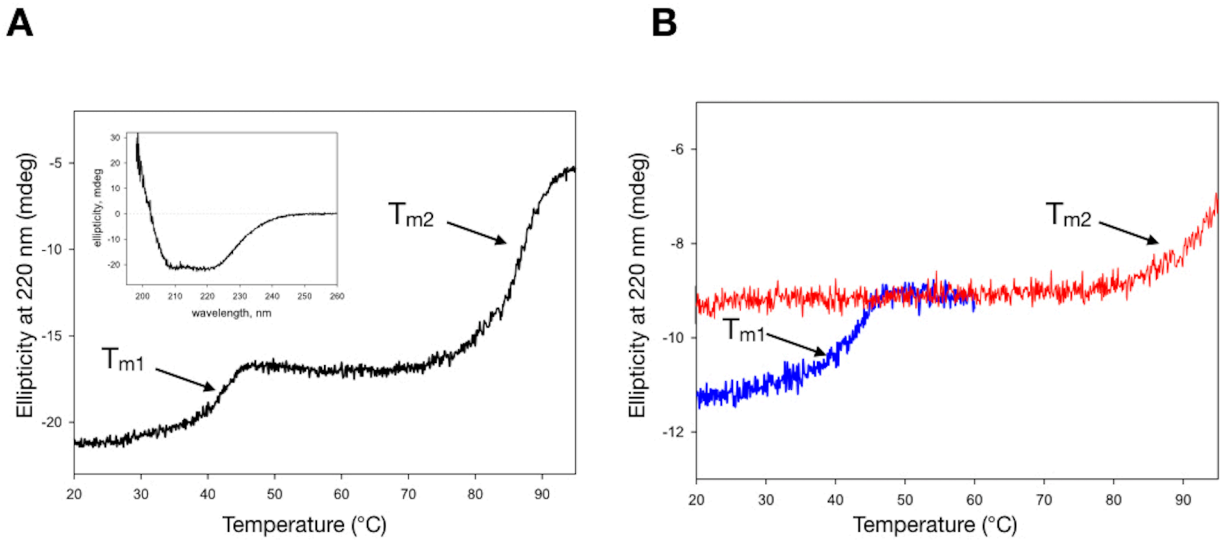

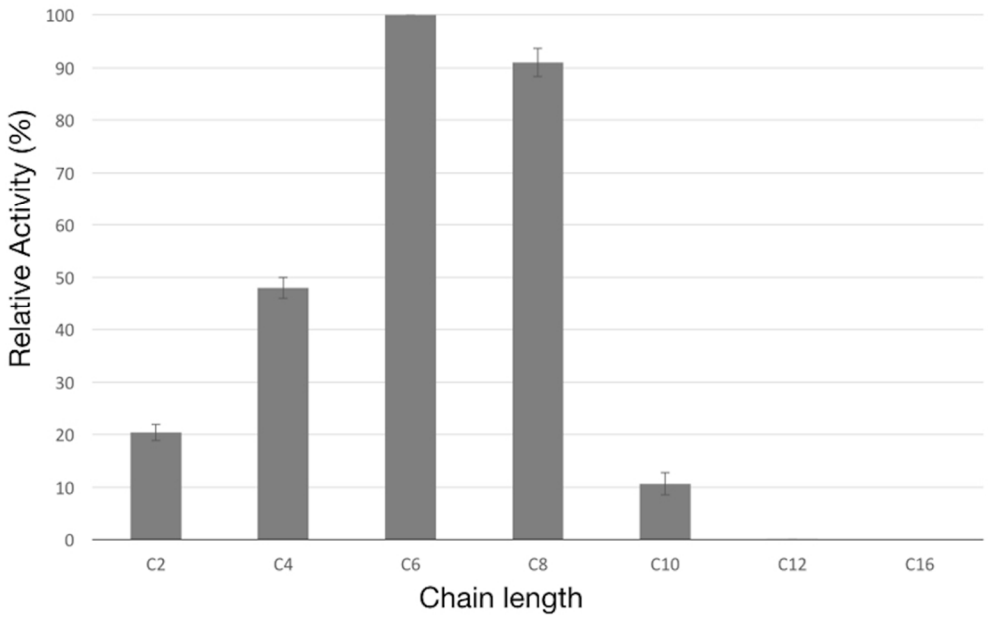

BCE activity towards *p*-nitrophenyl esters. Relative activity refers to the activity in the presence of *p*-nitrophenyl caproate (100%), and represents the arithmetic mean and standard deviation (SD) of three measurements.

80x49mm (300 x 300 DPI)

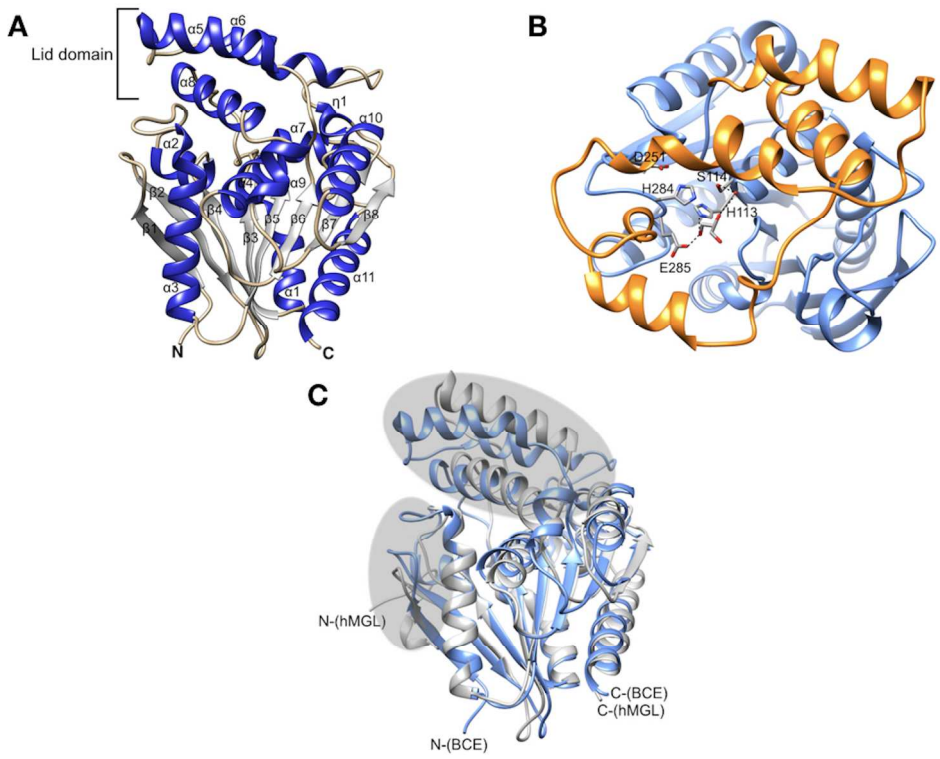

Figure 2. The crystal structure of apo-BCE and structural comparisons with hMGL. (A) Ribbon secondary structure representation of the crystal structure of apo-BCE. α-helices (blue) and β-strands (grey) and the N- and C-termini are labeled. The lid domain comprising α-helices 5, 6 and 8 is indicated. (B) View of the interaction between glycerol and BCE residues H113, E284 and a conserved water molecule (W27); hydrogen bonds are indicated by dotted lines. Interaction residues and catalytic triad (S114, H284, D251) residues are labeled and shown as sticks. (C) Superposition of the crystal structures of apo-BCE (blue) and inhibitor-bound hMGL (grey; PDB entry 3JWE, [28]). Structural variations are highlighted in shading. All figures were generated using Chimera [43].

165x123mm (300 x 300 DPI)

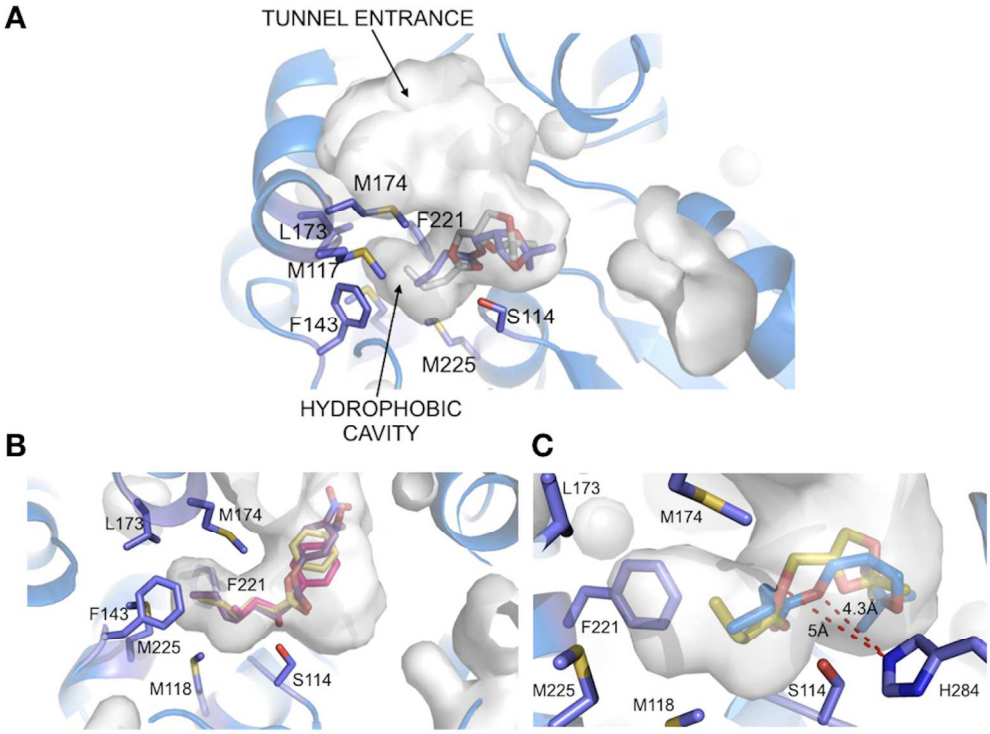

Analysis of the BCE substrate-binding site. A) Detailed view of the apo-BCE active site, highlighting the active site tunnel (surface representation); the entrance to the tunnel and the hydrophobic region of the active site are indicated. Hydrophobic residues, the catalytic S114 and the *R*- and *S*- enantiomers of butyrate-IPG (sticks) that were in silico docked to the active site are shown; B) in silico docking of p-nitrophenyl compounds (sticks) with different acyl chains of variable lengths; C2 (pink), C4 (ochre) and C6 (purple); C) Illustration of the bond distances between the substrate ester O atom and H284 NE atom in *R*-(yellow) and *S*-(blue) butyrate-IPG. Docking was carried out using Autodock4.2 [42].

165x123mm (300 x 300 DPI)

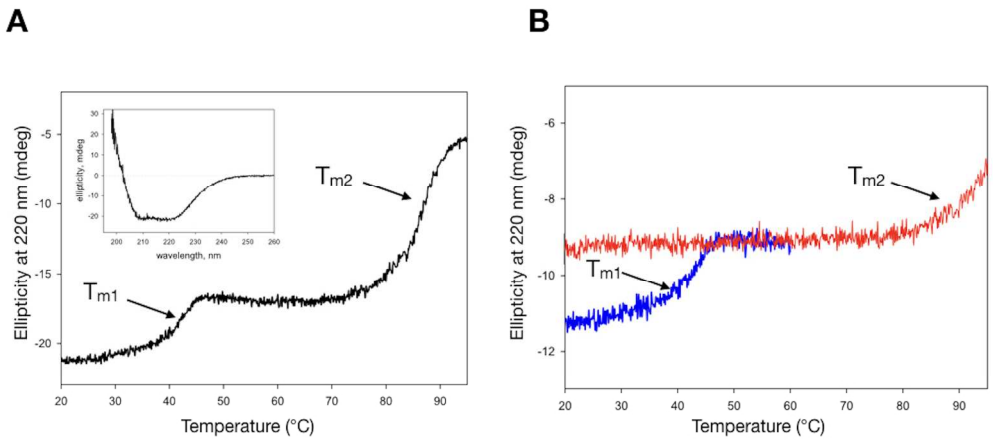

Conformational stability of BCE. (A) Thermal unfolding of BCE monitored through far-UV CD at 220 nm, as described in the Experimental procedures. The two transitions are labeled T_{m1} and T_{m2}, respectively. Inset: BCE far-UV CD spectrum; (B) the reversibility of the first conformational transition was evaluated by thermal unfolding of BCE, monitored through far-UV CD at 220 nm at protein concentration of 0.1 mg/mL. BCE was heated from 20°C to 60°C (blue line) and then cooled down to 20°C The same sample was heated up to 95°C (red line). The two transitions are labeled T_{m1} and T_{m2}, respectively. In this experiment, T_{m2} occurs at higher temperature due to the lower protein concentration.

163x77mm (300 x 300 DPI)